The International Journal of Advanced Manufacturing Technology
https://doi.org/10.1007/s00170-024-13739-w

ORIGINAL ARTICLE

Digital twin model of a large scale hot molten metal ladle pouring system

Ivan Popov[1] · **Christian A. Griffiths**[1]

Received: 22 January 2024 / Accepted: 2 May 2024

Abstract
In steel-making processes, large quantities (frequently exceeding 300 t) of liquid metal are transferred between vessels. In Basic Oxygen Steel (BOS) making process, metal is poured from Hot Metal (HM) ladles, utilising overhead gantry cranes, into furnaces for further processing. Due to the large quantities of liquid metal poured, this operation poses significant safety concerns associated with metal spillage and releases of heat emissions. This can further lead to damage being caused to surrounding infrastructure. Pouring automation can reduce the likelihood of metal spillage, optimising ladle movement for reduction in heat emission releases. Given the hazardous nature of this operation, robust testing and evaluation of automated crane pouring movements is required prior to their application. A digital twin (DT) model of an overhead gantry crane/HM ladle system is presented here, intended to provide a safe testing environment for controlled pouring movement and serve as a testbed for control system design studies. Accurate crane movement is achieved using multi-body dynamics, solving for non-linearities present due to rigid joint frictional components. The flow rate of HM is estimated through the application of a dynamic model, allowing the modelling of system dynamics due to differences in HM pouring weights. The devised DT model is evaluated by simulating real crane movement and making a comparison on the resultant changing HM weight inside the ladle. The devised DT removes the need for construction of a physical model or performing tests directly on the HM pouring system.

Keywords Basic oxygen steelmaking · Hot metal pouring · Digital twin · Friction estimation · Flow estimation · Multi-body dynamics · Dynamic system

1 Introduction

The pouring of Hot Metal (HM) in large quantities is carried out in heavy industrial processes. For example, in manufacturing of steel using Basic Oxygen Steel (BOS) process, where oxygen is blown at supersonic speeds into a liquid iron and metallic scrap melt to create steel. Here, these steel-making furnaces are "charged" with liquid iron, by pouring it from specially designed HM ladles, with amounts of HM exceeding 300 tonnes. Other examples where similar amounts of liquid metals are poured include charging of Electric Arc Furnaces (EAF) and the transfer of liquid steel from ladles to tundishes of Continuous Casting Machines. With transfer and pouring of such large quantities of liquid metal, the risks associated with metallic spills are amplified.

Molten iron and steel, charged inside BOS furnaces and, in some instances, EAF's, will reach temperatures in the excess of 1300 ^{o}C when poured. This process will release significant amount of thermal energy in the form of metallic fumes and flame. The diagram of HM charging, displaying the release of a flame front, is shown in Fig. 1. Typically, scrap is initially charged inside the furnace vessels. This will exacerbate these releases, due to impurities being burned off from the scrap surface. The presence of moisture in the scrap will further accelerate this, where water will rapidly expand to form superheated steam. Prolonged exposure to these thermal releases can damage surrounding plant infrastructure [1–3], leading to production delays to undertake necessary repairs. Although the causes for these heat emissions are widely known, little prior research has been carried out in trying to quantify these with different process factors. It is presumed that the release of these emissions is related

✉ Ivan Popov
708967@swansea.ac.uk

[1] Faculty of Science and Engineering, Swansea University, Swansea SA1 8EN, UK

Published online: 16 May 2024

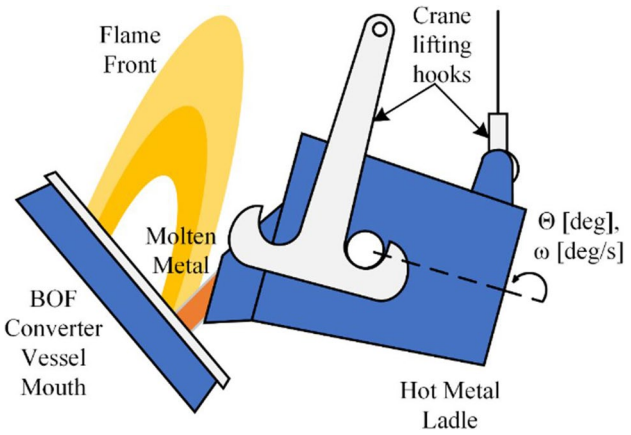

Fig. 1 Illustration of HM charging into a BOS converter vessel with release of a flame front

to the manor of how the liquid metal is charged, typically leading to the creation of site-specific guidelines that govern allowable pouring rates and pouring distances.

In these operations, HM is transferred and charged via the use of overhead gantry cranes or more often called, charging cranes. These lift the ladles via suspended hooks, whereby the elevation of which performs the tilting and, hence, pouring action. Since the introduction and industrial development of these steel manufacturing processes in the middle of twentieth century, the charging of liquid metal inside steelmaking furnaces has largely remained a manually operated process. Although automation attempts exist, predominantly, this is carried out by relying on the skills and precision of crane operators. With any manual tasks, human error factor will always be present. This, in turn, introduces process safety concerns, leading to possibilities of miss-pouring and metallic spills.

The manner in the way HM is poured can influence the release of hot metallic fume and dust emissions [4–6], introducing a further shortcoming with manual pouring operations. Here, it can be challenging for the crane operators to maintain sufficiently low pouring rates and distances to the mouth of the furnace, to minimise the release of these emissions. This can lead to process variations, depending on pouring behaviours of individual crane operators, leading to different pouring times. This can pose further planning challenges in these heavily organised industrial operations. One way to overcome these challenges is through the automation of this charging process; enabling close pouring positional and flow rate controls, ensuring predictable pouring times with each consecutive HM charge. These areas of research have been widely explored in metal foundry and casting industries. Here, precise flow rate and liquid stream position control are required to reduce the likelihood of casting defects. Example applications of flow rate controls for casting pouring machines can be found in [7–14] and accurate pouring position controls in [8, 13, 15–17].

Crane automation is not a novel concept, being widely researched for industrial applications (autonomous load pick-up, transportation and placement) [18–26]. However, automation of charging cranes to enable autonomous pouring of liquid metal is yet to become common practice. A single example is found in the literature [27], where a reference feed-forward speed control signal is developed to control the elevation of an auxiliary lifting hook on a charging crane, used in HM pouring operations. This speed estimation model was created in MATLAB [28] and is based on the geometry of the HM ladle. However, the authors provide no validation results and prior testing before applying this automated pouring scheme on the charging crane.

Given the scale of the operation and the amounts of liquid metal being poured, concern arises in applying automated pouring directly on to the charging cranes, without prior robust testing and evaluation of automated pouring movement controls. Lack of such testing can lead to serious process safety incidents. In examples [9, 11, 13, 16, 17], the developed automated pouring controls were validated using physical laboratory models and a safe pouring medium (i.e., water). However, creation of a physical pouring model for a HM charging system, utilising a gantry charging crane, can be expensive and impractical if a full-scale model is required. Due to safety concerns, testing of the resultant models with HM would not be permitted. Although testing with safer alternative pouring mediums is possible, these do not accurately translate the dynamic behaviour of liquid metal.

Software-based models, specifically those utilising Multi-Body Dynamics (MBD), have been widely used for testing and evaluation of rigid mechanical systems. MBD modelling allows for creation of simulations, where resultant interaction forces between different model body components can be evaluated. These can be studied through coupling of body components via the use of different connective joints (e.g., prismatic, revolute and spherical); defining movement and specifying constraints (e.g., friction, damping, contact forces and movement limits). In MBD simulations, equations of motion are solved for each body component and for coupled interactions between them, at each computational iteration. Modern MBD simulation packages will establish and solve system equations of motion, based on geometry and mass information of components. The use of these has been found in many fields, including heavy industries, construction, automotive and domestic [29]. The purpose behind carrying out MBD simulations can also differ on a case-by-case basis. Specific to crane and lifting systems, these include but are not limited to creation of a digital environment for testing of new and existing products and installations [30, 31], control system design and testing [32], online system

parameter identification [33], trajectory planning visual aid and operator training simulation software [34, 35].

The creation of a software-based digital twin (DT) of the HM charging system, capable of accurate replication of crane/ladle movement and prediction of resultant HM flow rate, would provide a safe and cost-effective means for testing and evaluating pouring movements, prior to their application on the actual process. Although application of HM pouring controls is not a novel concept, with examples seen applied to similar HM charging operations, the creation of DT's for testing and evaluation of such systems has not been found in the literature, identifying a gap in research. In this paper, a novel approach for testing large-scale HM pouring systems through the application of a DT is presented. Here, by accurately modelling mechanical system movement, HM ladle pouring rates can be predicted and used for testing and evaluation purposes.

The following section establishes the design of the MBD model for the HM pouring system. Here, emphasis is made on non-linear frictional torque generation between revolute joints, providing movement damping during ladle tilting motion. Section 3 presents static and dynamic frictional torque estimates and their adaptation in a velocity-based real-time friction estimation model, integrated to provide feedback to revolute joint blocks within the MBD model. Section 4 constructs a dynamic system model for fluid flow estimation, based on Bernoulli principles and considering HM ladle geometry. Here, fluid flow is estimated based on ladle position and radial velocity, extracted at each simulation step from the MBD model. Methodology for evaluating the performance of the combined DT model, comprising of the MBD, velocity-based friction estimation and fluid flow prediction models is established based on simulation of real crane/ladle movement and comparison of changing load weight during HM pouring, between real and simulated results. This evaluation is performed in Sect. 5. Finally, conclusions are made on the performance of the devised DT model and its practical applications.

2 Methodology

2.1 Description of hot metal charging system

The pouring system, for charging of BOS converter vessel with HM comprises of a heavy-duty lifting gantry crane and a HM pouring ladle. These cranes typically have 3 degrees of movement: long-travel, short-travel and hooks hoisting operations. Long-travel allows the crane to move along the length of the plant, via a suspended rail mechanism. Cross-travel allows for crane "trolleys", which house mechanisms for hoisting main and auxiliary lifting hooks, to move perpendicular to long-travel movement. HM charging cranes use two of such trolleys: main trolley and auxiliary trolley, housing main and auxiliary lifting hooks mechanisms, respectively. The final degree of movement involves vertical movement of the lifting hooks, performed via hoisting of the lifting cables via hoisting drums, through a system of effort-reducing pulleys. The full crane system is displayed in Fig. 2.

2.2 MBD model

In this work, MATLAB Simulink [36], using Simscape [37] and Simscape Multibody [38] libraries of components were utilised. This package was chosen due to a wide variety of build-in tools and the ability to integrate MBD models. The model of the crane was simplified, utilising only those mechanical subsystems that are involved in the HM charging movement. This was done to reduce the number of model components, improving efficiency and computational times. To further simplify MBD model creation, subassemblies were created using SolidWork [39], using CAD crane parts provided by the manufacturer. Here, rigid joint connections were specified and movement constraints were applied. Using a translation tool [40], resultant subsystems were then translated into MBD models within the Simulink environment.

These subsystems are as follows: (1) main lifting Trolley and main hooks hoisting mechanism, (2) auxiliary lifting trolley and auxiliary hoisting mechanism, (3) main hooks lifting boom and pulley mechanism and (4) auxiliary lifting hook and pulley mechanism. Subsystems 1 and 2 are displayed in Fig. 3a and b, respectively. The combined model is displayed in Fig. 4a and b, incorporating a model of a HM ladle. Here, subsystems 3 and 4 can be visible. It should be noted that only an overview of the MBD model setup is

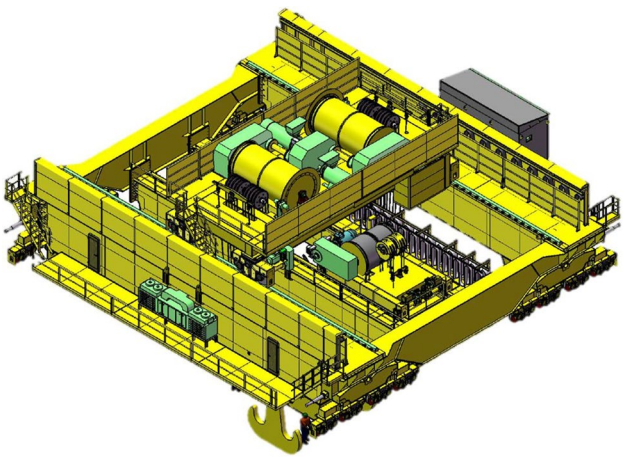

Fig. 2 Heavy-duty HM charging crane CAD model

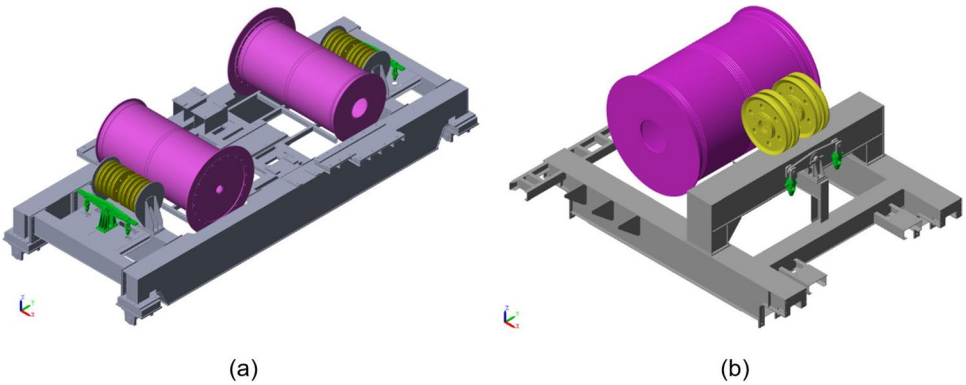

Fig. 3 Simplified MBD models of: **a** main lifting trolley, **b** auxiliary lifting trolley

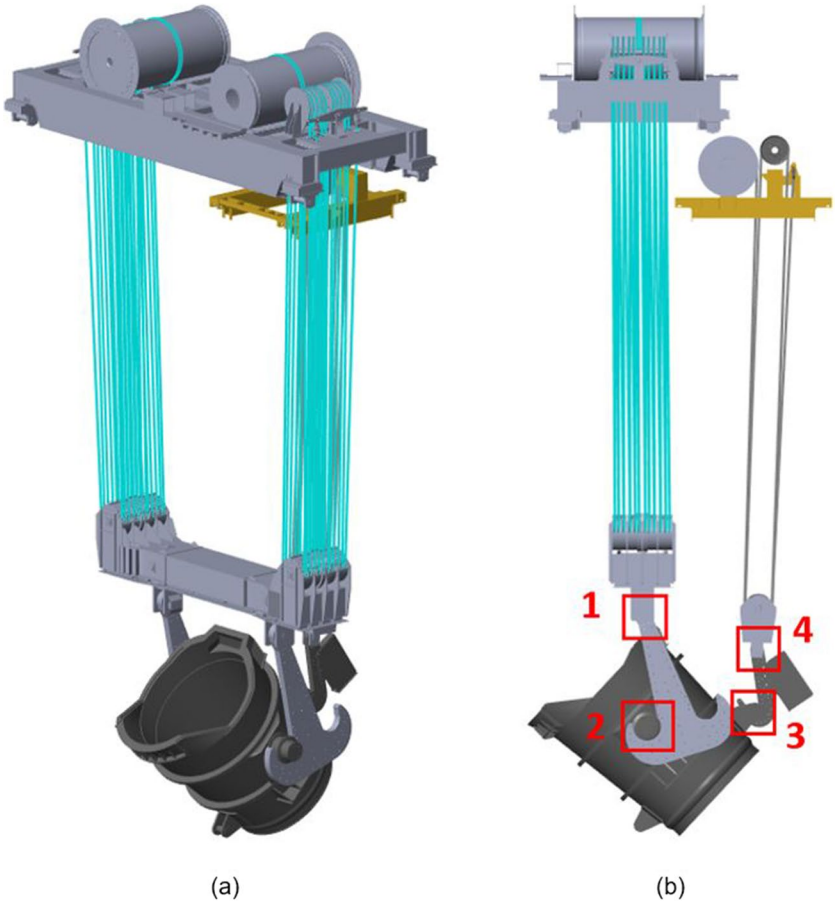

Fig. 4 Simplified MBD HM charging model. **a** Isometric profile, **b** side profile

provided here, since, using modern industry standard modelling software, this can be seen as a trivial task.

2.3 MBD model frictional torque estimation

Friction is a phenomenon that occurs in all mechanical sliding or rotating components, due to tangential reaction between two surfaces. This introduces resistive forces that oppose the direction of motion. It is vital that these resistive forces are considered in the design of MBD models, to provide an accurate system representation. This is especially important when design of a control system is considered, where friction will introduce opposing force moments that work against applied actuation forces. In the creation MBD model of the HM charging system, only the friction at the "load end" revolute joint components were considered. These provide a rigid connection between the following components: (1) main hook — crane boom, (2) ladle trunnion pins — main hooks, (3) ladle auxiliary lifting pin — auxiliary lifting hook and (4) auxiliary lifting hook – auxiliary pulley housing load block. These joints are illustrated in Fig. 4b, showing the corresponding joint identification

number. Due to utilisation of Variable Frequency Drives (VFD), the inclusion of friction components for other rigid and prismatic joints (for example, hoisting cable system pulleys and horizontal trolley cross-travel movement) was not considered. The VFD's control speed of movement by compensating for torque generation. This includes "back" torque generated due to joint friction.

Several friction models have been created and adapted for use in control system design and simulation modelling [41–43]. One of the earliest adopted models, used to describe rotational frictional torque, was presented by Coulomb [44] and is aptly named after its creator. This model, in its simplest form, relates frictional force to sliding velocity of the two bodies, coefficient of friction and normal force acting on the bodies. One drawback with utilising Coulomb's model is that it does not consider the effects of static friction (or stiction), when the two surfaces are at rest. In addition, velocity is not factored in calculation of frictional forces, which could lead to computational drawbacks [45]. To address drawbacks with the Coulomb model, concerning static friction, several models have been proposed in the literature. Examples can be found in [46–48]. These account for the Stribeck effect, where static friction is higher than the maximum dynamic friction and sees an exponential decrease from static to dynamic friction with increasing velocity. A recently proposed model by Brown and McPhee [45] has been developed to be used in a number of applications, including real-time simulations and multibody modelling. The advantage of this model is that it relies on physically meaningful elements only for the estimation of friction torque. This model can be illustrated using the following equation:

$$F_T = F_C tanh\left(4\frac{v}{v_d}\right) + \left(F_S - F_C\right)\frac{v/v_d}{\left(\frac{1}{4}\left(v/v_d\right)^2 + \frac{3}{4}\right)^2} \quad (1)$$

where F_T is the resultant frictional torque, v is the velocity of the joint, v_d is the velocity tolerance (at which maximum frictional force is applied), and F_C and F_S are the Coulomb and Stribeck friction terms, respectively.

From comparative analysis in [42], this model was shown to be suitable when used in friction estimation tasks; due to its ability to accurately capture static and dynamic friction characteristics, its reliance on few parameters for estimation and overall good computational efficiency results. For these reasons, and its non-reliance on physically meaningful elements, this model was chosen in this work for modelling of frictional torque in revolute joint components.

2.4 Coulomb and Stribeck terms estimation

Authors in [49] provide detailed calculations and analysis in estimating Coulomb (and Stribeck) friction for revolute joints, based on elasticity and radial stress of the joint components. An estimation equation is formed, based on equilibrium equations for stress distributions between cylindrical contact surfaces of revolute joint component. The following Eq. (2) is the simplified form of this resultant:

$$F_C, F_S = FRC_\alpha \frac{\mu}{\sqrt{1+\mu^2}} \quad (2)$$

where

$$C_\alpha = 1 + 0.0477k^2 + 0.5744k^4 - 1.051k^6 + 0.6982k^8$$
$$k = \sin\alpha$$

In Eq. (2), F is the normal force applied on the joint, R is the radius of the inner revolute joint component, μ is the coefficient of friction between the materials of the joint component surfaces and α is half of the maximum angular contact. It should be noted that for estimation of Coulomb or Stribeck friction is performed by substituting corresponding dynamic or static coefficients of friction μ.

To estimate F_C and F_S, resultant contact angle between revolute joint components is required. Methodology for estimation of this contact angle is also provided by authors in [49]. Here, this angle can be estimated knowing the elasticity, coefficient of friction, applied force and outer and inner geometry of the joint components. This estimation is carried out using the following equation:

$$\alpha = \sin^{-1}\left[\sqrt{\left(\frac{2.31F_n}{Eb\sqrt{1+\mu^2}} \cdot \frac{R'/R}{R'-R}\right)}\right] \quad (3)$$

where E is the modulus of elasticity of the two joint component materials and b is the length of the joint. In instances where two different materials are used in the joint, Eq. (4), can be applied to estimate the combined modulus of elasticity E [49, 50]:

$$E = \frac{1.82E_1E_2}{\left[\left(1-\nu_2^2\right)E_1 + \left(1-\nu_1^2\right)E_2\right]} \quad (4)$$

where E_1, E_2, ν_1 and ν_2 are the modulus of elasticity and Poisson's ratios for the two joint components, respectively.

2.5 Velocity-based friction model — MATLAB simulink implementation

The guide provided in MATLAB [51] specifies friction modelling of revolute joints. However, this "best practice" method does not account for application of variable forces required here, due to significant changes in load mass, with HM being poured out of the ladles. This applied force changes as a function of ladle rotation angle θ. Therefore, a custom method was applied in MATLAB Simulink environment for the estimation of frictional torque. A revolute joint friction estimation model was developed based on

mathematical Eqs. (1)–(4). The following steps are utilised in estimating frictional torque for revolute joints: (1) Estimate force acting on the joint due to changing ladle mass (as a function of rotation angle θ), (2) Calculate dynamic (Coulomb) and static (Stribeck) friction and (3) Perform velocity-based frictional torque estimation, using (1).

2.6 Joint force estimation

Force acting on the joints is taken as that of the force due to weight of the HM contained inside the ladles and the weight of the load structure (i.e., the HM ladle and lifting hooks). With ladle engaged by both Main and Auxiliary lifting hooks, the weight of the load and, hence the resultant force applied at each revolute joint, will be distributed accordingly. Here, a type 2 lever mechanism is formed. During ladle tilting, the centre of mass of the ladle and HM will lie between the lifting point (Auxiliary lifting hook) and the fulcrum (Main lifting hook). The weight will therefore be shared between these lifting hooks. This can be illustrated using Fig. 5.

With ladle rotation, and hence subsequent pouring of the HM, the force acting on these hooks will change. Estimation of the force required to tilt the ladle, using the auxiliary lifting hook, can be established based on the force moments acting on the auxiliary hook during ladle rotation. This estimation is carried out in two stages: (1) calculation of the moment due to changing weight of the liquid inside the ladle and (2) calculation of the moment due to the mass of the empty ladle [52]. The required lifting force is then estimated using the combined force moment and geometric information about the ladle, using Eqs. (5)–(8) [52]:

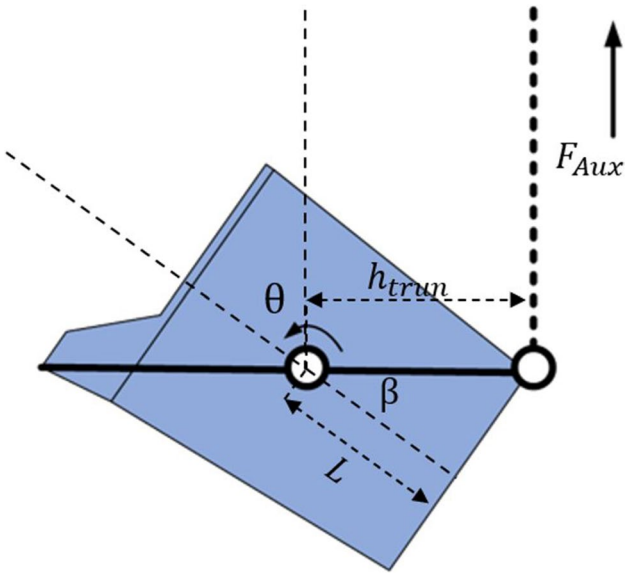

Fig. 5 Resultant type 2 lever, consisting of HM ladle and auxiliary lifting mechanism

$$F_C = F_{HM} + F_L \tag{5}$$

$$F_{HM} = \rho g V\left[\left(h_{trun} - y_l\right)\sin\ \theta - x_l \cos\ \theta\right] \tag{6}$$

$$F_L = m_k g\left(h_{trun} - y_k\right)\sin\ \theta \tag{7}$$

$$F_{Aux} = \frac{F_C}{L\ \sin(\theta+\beta)} \tag{8}$$

where F_C is the combined force moment acting on the Auxiliary hook, F_L is the force moment due to weight of the liquid metal, F_{HM} is the force moment due to the weight of the ladle, ρ is the density of liquid metal, g is the gravitational potential energy, V is the volume of liquid in the ladle, h_{trun} is the height of trunnion pin from the bottom of the ladle, y_l and x_l are the vertical and horizontal positions of the centre of mass of the liquid metal, θ is the angle of rotation of the ladle, M_k is the force moment due to the weight of the ladle, m_k is the empty ladle weight, y_k is the vertical centre of mass coordinate of empty ladle, F_{Aux} is the force acting on the lifting hook, L is the distance between trunnion pin and aux. hook connection with the ladle and β is the vertical angle between trunnion pin and aux. hook connection point.

The force acting on the main hook, during ladle rotation can be estimated using the following:

$$F_M = g\left(\frac{M_{Lad}+M_{HM}(\theta)}{2}\right) - \frac{F_{Aux}}{2} \tag{9}$$

where F_{Mhook} is the force acting on the main hooks, M_{Lad} is the mass of the empty ladle and M_{HM} is the mass of the HM.

For revolute joints 2 and 3, forces F_M and F_{Aux} are used, respectively. For joints 1 and 4, the weight of the main and auxiliary lifting hooks, respectively, are included in the estimation of resultant forces. For joint 1, (9) is modified to include the weight of the main hook, resulting in:

$$F_{MBoom} = g\left(\frac{M_{Lad}+M_{HM}(\theta)}{2} + M_M\right) - \frac{F_{Aux}}{2} \tag{10}$$

where F_{MBoom} is the resultant force applied at joint 1 and M_M is the weight of main lifting hook.

To find resultant force on joint 4, force due to the weight of the auxiliary hook is simply added to F_{Aux} in Eq. (8).

3 Friction results and estimation model implementation

3.1 Coulomb and Stribeck friction

For the estimation of Coloumb and Stribeck friction, as a function of ladle rotation θ, Eqs. (2)–(4) were used and Eqs. (8) and (9) for estimation of forces acting on the

Table 1 Joint information used in frictional components estimation

Model component	Joint 1	Joint 2	Joint 3	Joint 4
Outer radiusR'(mm)	133.5	393	127	101.55
Inner radius$R$(mm)	133.35	381	114.5	101.5
Joint length$b$(mm)	255	255	273	222
Staticμ	0.15	0.35	0.35	0.15
Dynamicμ	0.08	0.35	0.35	0.08
Effective$E$(GPa)	210	140	140	210
Velocity coefficient v_d	1e-3	1e-3	1e-3	1e-3
Contact angle$\alpha(\theta = 0)$, Staticμ	55.9	6.64	0.77	10.9
Contact angle$\alpha(\theta = 55)$, Staticμ	37.32	4.43	3.36	55.59
Contact angle$\alpha(\theta = 90)$, Staticμ	28.94	3.38	0.75	10.51
Contact angle$\alpha(\theta = 0)$, Dynamicμ	56.3	6.64	0.77	10.94
Contact angle$\alpha(\theta = 55)$, Dynamicμ	37.5	4.43	3.36	55.92
Contact angle$\alpha(\theta = 90)$, Dynamicμ	28.9	3.38	0.75	10.55

Table 2 Information used in auxiliary lifting hook effective force estimation

ρ (kg/m^3)	g (m/s^2)	m_k(kg)	L(mm)	β(deg)
6900	9.8	138,600	3673	52

joints. The 4 joints differed in terms of their geometries and construction: joints 1 and 4 are fully enclosed joints and 2 and 3 are semi-enclosed. Different materials were also used in their constructions: Joints 1 and 4 resulted in a steel-steel contact and joints 2 and 3 in a phosphor-bronze on steel contact (here a phosphor-bronze wear pads are used in the construction of the lifting hooks). Table 1 displays information used in estimation static and dynamic friction components. The values for static and dynamic μ are found in [53, 54], for construction materials used. Effective E was estimated using values found in [55]. It should be noted that for contact materials in joints 2 and 3, results in equal static and dynamic μ. To estimate the effective force applied at the auxiliary lifting hook, information displayed in Table 2 is used. The centre of mass coordinates of the empty ladle and HM contained within, can be estimated using methodology outlined in [52]. However, this information was acquired directly from the ladle manufacturer. Here, the centre of mass values did not account for potential ladle refractory degradation or slag adhesion that would result in marginal changes in centre of mass location. This would only cause small weight deviations in comparison to overall weight of the ladle and HM held within, therefore, these marginal changes were deemed not critical to the performance of the model.

The HM density value ρ in Table 2 is a generalised value, used based on the typical grades of steel produced at this plant. Depending on the HM chemistry, this value can fluctuate marginally with each HM charge.

The results in Fig. 6 display static and dynamic frictional torque generation for joints 1–4, as a function of ladle rotation angle θ (measured between 0 and 90^o). Here, it should be noted that due to equal static and dynamic friction coefficient values in joints 2 and 3 result in equal Coulomb and Stribeck friction components.

3.2 Velocity-based revolute joint friction estimation model

Frictional torque estimation, as a function of joint velocity, for the 4 outlined revolute joints was estimated using model displayed in (1). This model was implemented in MATLAB Simulink environment, where live model frictional torque estimation was performed based on Ladle position and joint velocity data, fed from the MBD model. Frictional torque estimates, displayed in Fig. 6 for joint 1, were used

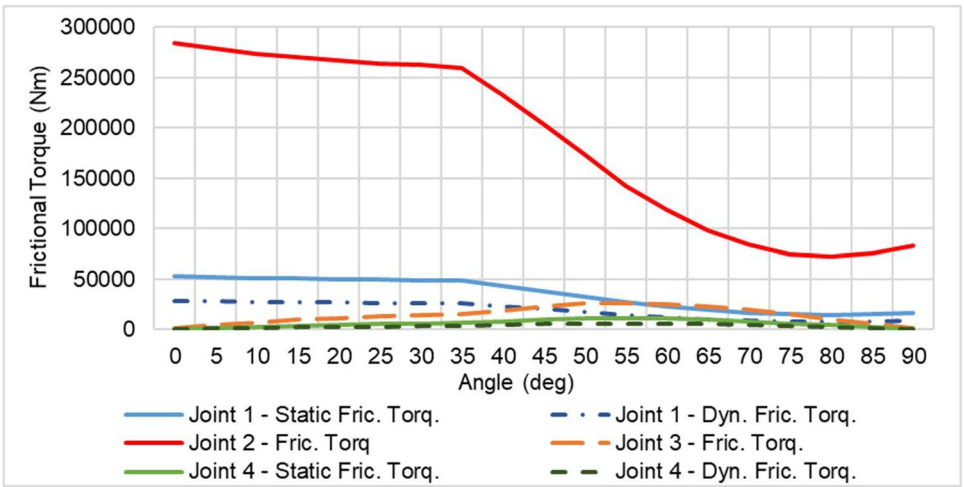

Fig. 6 Frictional torque estimation with ladle rotation

as look-up tables. Figure 7 displays model constructed for estimation of frictional torque for joint 1. Due to limitation in using hyperbolic function within the MATLAB function block, to estimate dynamic friction term of the velocity-based model in (1), a separate subsystem was constructed within the Simulink environment, splitting this model into Static and Dynamic friction components. Model set-up for joint 4 is identical to the one displayed in Fig. 7, except for utilization of static and dynamic friction for that joint from Fig. 6.

In estimation of velocity based frictional torque for joints 2 and 3, Dynamic frictional component was used only. Example setup for joint 2 in MATLAB Simulink is displayed in Fig. 8.

Frictional torque estimates from these models are then subsequently fed back to the relevant revolute joint blocks as torque input signals in the MBD model.

4 HM flow rate estimation dynamic system model

In this work, flow rate estimation was based on work presented in [9, 11, 14]. Here, flow rate estimation is based on application of Bernoulli hydro-dynamic principles for fluid flow. Dynamic equations are set creating relationships between the hydro-dynamic principles, liquid pouring rate, geometry of main ladle body and the shape of the pouring mouth. To summarise, pouring rate is estimated based on the evaluation of the rate of change in the height of liquid and surface area that is present above the pouring mouth, during rotation of the ladle. This is illustrated in Fig. 9, where $A1$, $A2$ and $A3$ are the surface areas of liquid metal above the pouring mouth and $h1$, $h2$ and $h3$ are the heights between liquid surface and the pouring mouth.

At each time iteration, height of liquid above the pouring mouth, will depend on ladle rotational speed. With slow speeds, the rate of change in the height of liquid above the pouring mouth will be small. Hence, this will result in low pouring rates. With faster speeds, the rate of change in liquid height will increase proportionally. This, in turn, will result in faster transfer of liquid from the ladle. The total liquid volume change (V_r) can be estimated by taking the volume bounded by the resultant liquid surface area (A_{surf}) and height of liquid (h).

The shape of ladles used in this process resemble that of a frustum of a cone. Height h and hence volume V_r can be deemed small in comparison to total ladle height and volume held within, with each time iteration. Therefore, additional volume in V_r, due to slanted ladle walls, can be seen as negligible. Here, the following identity will apply:

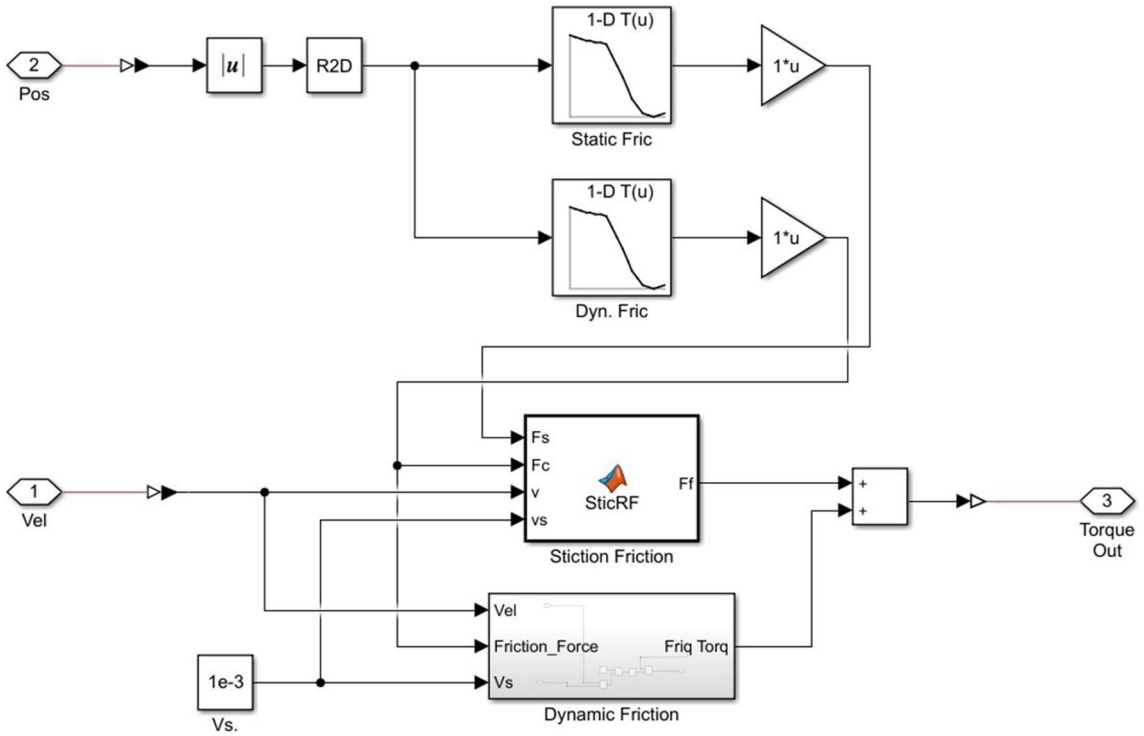

Fig. 7 Velocity-based frictional torque estimation model for revolute joint between main lifting hook and crane boom, constructed in MATLAB Simulink

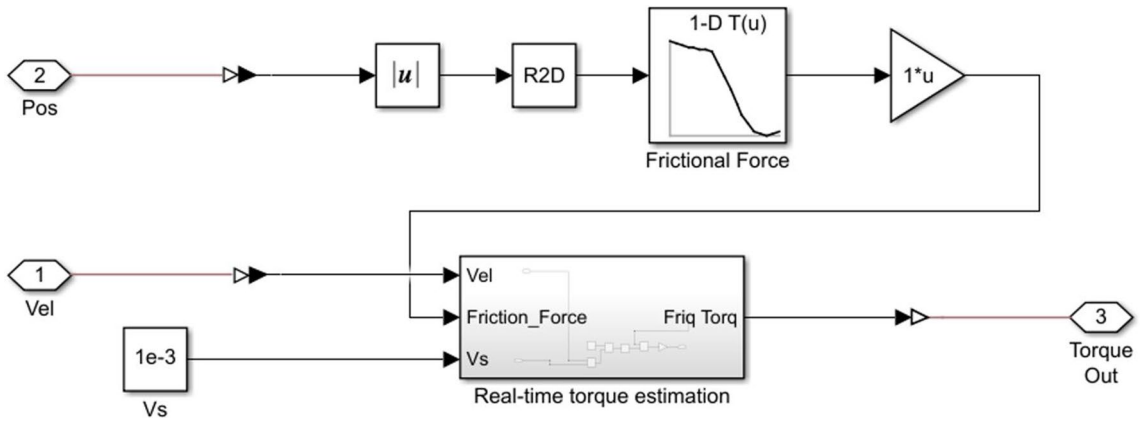

Fig. 8 Velocity-based frictional torque estimation model for revolute joint between main lifting hook and HM ladle, constructed in MATLAB Simulink

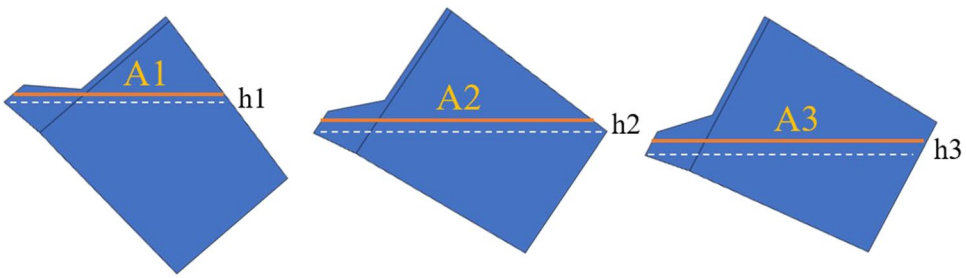

Fig. 9 Changes in liquid surface area and height of liquid above the pouring mouth, with rotation of the ladle

$$h(t) \approx \frac{Vr(t)}{A_{Surf}(\theta(t))} \tag{11}$$

Volumetric change V_r can be estimated by relying on a relationship between liquid flow rate q and the change in total liquid volume V_{lad}, at each time iteration [9]:

$$dV_r(t) = -q(t) - dV_{lad}(t) \tag{12}$$

where V_r is then found by performing integration.

The flow rate of liquid leaving the ladle will depend on the liquid channel area projection, created by the shape of the pouring mouth. This is illustrated in Fig. 10.

The resultant dynamic Eq. (13) [9, 11, 14], equates liquid pouring rate to changing heights of liquid metal above the pouring mouth as a function of liquid flow channel projection area:

$$q = c \int_0^{h(t)} \sqrt{2gh}\, dA_M \tag{13}$$

where q is the flow rate, c is the flow resistance coefficient and A_M is the flow channel projection area. The flow resistance coefficient c is a value between 1 and 0 that translates resistance due to shape of the ladle, ladle material and the viscosity of fluid medium. This value is determined through experimentation [11], by comparing model results to actual pouring results from the real system.

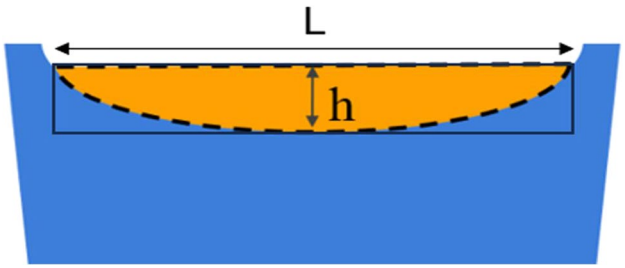

Fig. 10 Liquid projection over pouring mouth

4.1 Pouring channel flow model considerations

The model uses a rectangular shape to estimate the liquid stream projection area, illustrated in Fig. 10. Here, the curvature of the pouring mouth is significantly large, therefore, the rational is that a rectangular shape would be

sufficient for providing a close approximation of the resultant liquid stream area projection. In addition, ladles are lined with refractory material. This material will degrade with prolonged use, causing deformation of the pouring mouth curvature. Previous examples in the use of rectangular pouring mouth estimation can be found in [11] and [13]. In [11], the area is simply estimated by varying the height of the resultant shape, while keeping the length of the flow channel a static value. A look-up table is used in [13], to estimate the length of the projected flow channel, as a function of height of liquid above the pouring mouth. A modification on this approach is employed in this work, where, instead of relying on the use of a look-up table, a numerical model is applied for channel length estimation.

When ladles are rotated, the shape of the pouring mouth resembles that of an elliptical segment. With HM flowing out of the ladles, the resultant area projection flow channel will also resemble an elliptical segment. Here, the channel length can be taken as the segment chord. The length of a chord can be estimated given the segment height and curvature radius [56]:

$$L_{Chord}(t) = 2\sqrt{h(t)\left(2R_{Lip} - h(t)\right)} \tag{14}$$

where L_{Chord} is the length of the chord and R_{Lip} is the radius of the pouring mouth curvature.

In (12), using the rectangular area projection model, A_M is taken as $L_{Chord} \times h$, where the resultant integration is then performed in respect to the height of the liquid h. By solving the resultant integration in (12) and then solving the subsequent simultaneous equation using (11) and (13), pouring rate q is found using:

$$q(t) = \frac{2cL_{Chord}\sqrt{2g}}{3A_{surf}(t)^{3/2}}\left(V_r(t)^{3/2}\right) \tag{15}$$

4.2 Flow rate estimation model

The model for estimating flow rate of liquid, as a function of ladle rotation θ, was constructed in MATLAB Simulink. Here, Eqs. (12) and (15) are solved, using ladle rotation reference signal θ from the MBD model. Look-up tables for volume of liquid inside the ladle V_{Lad} and surface area of liquid A_{Surf}, as functions of ladle rotation angle θ, are used as further inputs to this model. These look-up tables were developed based on the geometry of the ladle and are displayed in Fig. 11. Here, 331.5 t HM amount was considered. Implementation of this model within the Simulink environment is shown in Fig. 12.

Ladle volume V_{Lad} and surface area of liquid A_{Surf} are tied to the geometry of the ladle. Refractory degradation and slag adhesion will alter the internal ladle dimensions. Varying these parameters to meet the conditions of the ladles would improve model accuracy. Often, only a periodic visual ladle inspection is carried out, making it difficult to estimate these non-linear dimensional changes. Due to this limitation, look-up data in Fig. 11 was constructed based on ladles with no internal degradation.

It should be noted that in Fig. 12 additional blocks are used: Angle Actual estimates combined ladle angle due to rotation of the ladle and main lifting hook. Volume limit prevents increases in volume due to reverse ladle rotation, extracted from the look-up table.

Liquid sloshing movement can occur due to rapid changes in ladle movement and vibrations that can impact the amount of HM being poured. This effect is most prevalent at the beginning of the pour, where ladle is moved into position and stopped over the converter vessel mouth, leading to inertial movement of the crane/ladle. Typically, some time is allowed prior to initiating pouring to allow for sloshing effect to reduce. During pouring, ladle rotation movement can be considered sufficiently slow and without rapid changes that could introduce significant inertial movement. Ladle back-tilting is also typically not expected. Therefore, modelling of liquid sloshing effects was not considered in this DT.

4.3 Model verification methodology

Verification of the flow rate prediction model was performed by making a comparison between simulated HM weight,

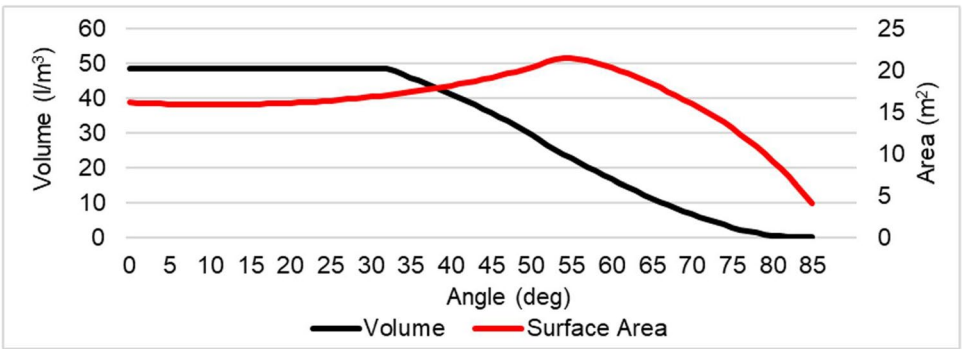

Fig. 11 Example data used in look-up tables, displaying liquid metal volume (black) and liquid surface area (red), as functions of ladle rotation angle θ

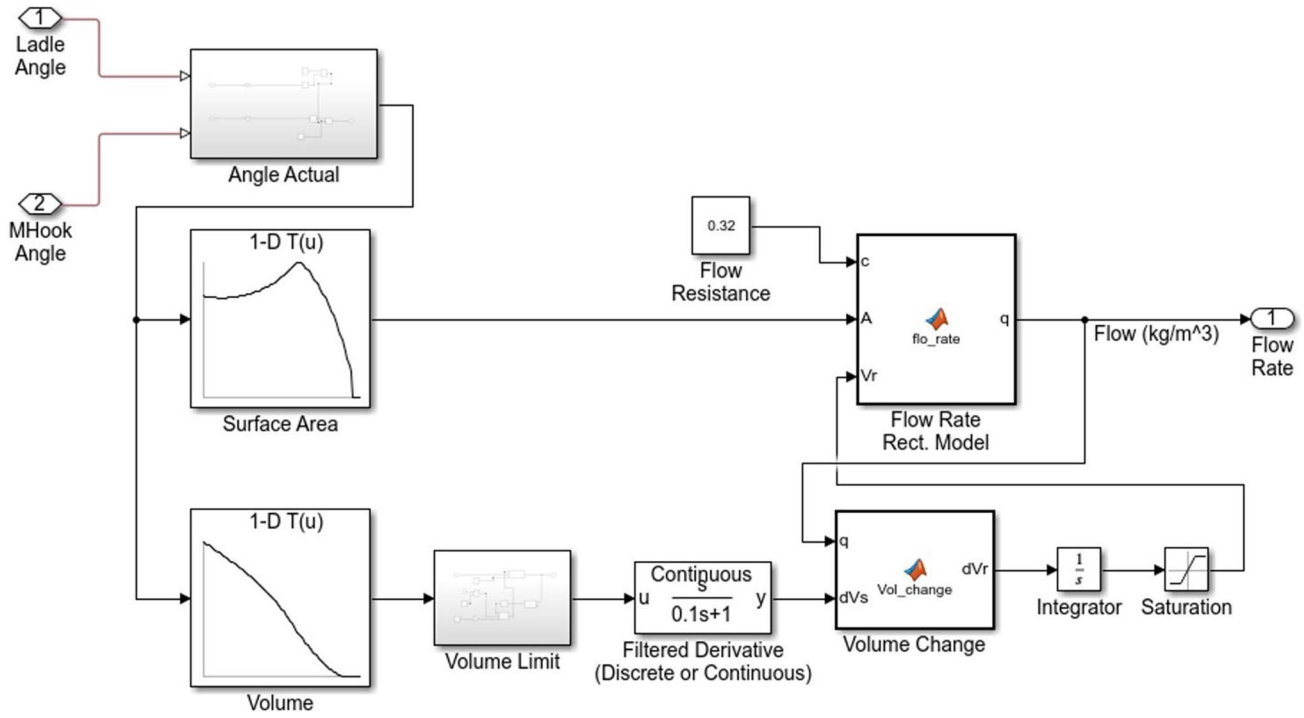

Fig. 12 Flow rate estimation model in MATLAB Simulink

Fig. 13 Example HM charging angle measurement at time t and t + n

estimated using the devised flow prediction and MBD models for the HM charging system, against actual process HM weight charging data. In total, ladle movement from 5 HM charges was replicated using the DT model. For each HM charge, simulations were repeated for a range of flow resistance coefficient values c. These range from 1 to 0.2, in 0.1 decrements and are carried out as a means of model calibration, by outlining most suitable value.

On HM charging crane, ladle weight is measured via load cells, installed on main and auxiliary lifting mechanisms. Here, changing weight of ladle and HM contained within is measured. Although it is possible to evaluate HM flow rate using this data, due to inertial movement of the crane during HM charging, these measurements can be susceptible to noise. Therefore, the changing HM weights are instead compared.

To record ladle movement, video recordings of the process were used. Here, a camera was placed adjacent to the HM charging process. Video frames were then segmented at 2 s periods and ladle angle was measured. Example frames from a single video are displayed in Fig. 13.

Due to an initial "free-hanging" ladle angle, a discrepancy exists. This means that when auxiliary hook is engaged with the ladle, to initiate ladle tilt, the ladle will not always measure 0^{o} on the vertical plane. This angle is present due to changes in the centre of mass, caused by: variations in HM pouring amounts, degradation of internal refractory materials and metal slag buildup inside and outside the

ladles. Therefore, it is difficult to accurately determine ladle position using main and auxiliary hook hoisting encoders, instead relying on estimation of ladle position through video recordings.

Based on this ladle angle rotation θ, an auxiliary hook hoisting velocity signal and hence auxiliary hoisting drum signal, in Revolutions per Minute (RPM), was constructed for each of the recorded HM charges. Reference movement signals for main and auxiliary cross-travel trolleys were constructed based on positional data extracted from crane movement encoders.

Using video recordings will only provide a close approximation of ladle position. A discrepancy can be present between actual and measured positions. This is due to the mounting position of the camera and lens distortion. The effect of this can be minimised by accounting for measuring angle of the camera and through application of image filters. Absolute position can only be measured by using encoders in both the ladle trunnion pin and main lifting hook, to record actual rotation of the ladle and offset angle due to main hook position. However, the installation of these encoders was not possible in this specific process.

5 HM charging model validation results and discussion

In Fig. 14a–e, a comparison is made between recorded HM charging weight of ladles and simulated results. Measured HM weight is displayed using a solid line, with simulated results displayed using a dotted line, for a range of different flow resistance coefficients c (1, 0.8, 0.6, 0.5, 0.4, 0.3 and 0.2). Here, changing weight is estimated by integrating the simulated flow rate results. It should be noted that the weight of empty ladles was deducted, displaying changing weight of HM only.

An error percentage between the measured weight value and the simulated results are calculated for the 5 performed tests. Table 3 displays this error between actual HM weight and simulated results. Here, flow constant values are displayed, which resulted in the smallest percentage deviation. Here, the weights of the empty ladles were included in this percentage error estimation.

From these results, the average error percentage between the actual process and simulated results for the 5 tests ranged between 3.19 and 4.79%, with an overall average of 4.1%. For this process, this error deviation can be seen as acceptable and deemed a good overall approximation of the HM charging process. Here, the requirement is to pour HM at sufficiently low rates [5], that would reduce the likelihoods of significant heat emissions. This simulation error does not pose a risk of significantly increasing the poured HM weight and hence causing rapid changes in HM pouring rates, that could influence the release of these emissions.

The flow resistance coefficients, which resulted in the smallest percentage error, for tests 1–5 were 0.4, 0.3, 0.2, 0.4 and 0.3, respectively, with an average of 0.32. These values, indicate presence of resistance to flow and are in line with values (<0.6) recorded in literature in [11, 13]. Model accuracy is dependent on the use of appropriate flow resistance coefficient c values, that accurately convey resistance to flow encountered due to ladle geometry, material properties, ladle and pouring mouth condition and HM viscosity. These process parameters are difficult to monitor in a live production environment and for each HM charge. Difficulty in estimating ladle refractory conditions, which will impact flow resistance, has been discussed previously. HM viscosity will depend on several factors, that include HM temperature, chemistry and metallic slag inclusions. It is currently not possible to use these parameters alone for prediction of flow resistance coefficients, which are estimated through experimentation only.

It should be noted that toward the end of each recorded HM charge, the model's ability to accurately simulate changing weight of HM and hence its flow rate decreases. Taking an average for the first 75% of the recorded HM charges, results in an average error of 2.12%. In Fig. 14a–e, from the point where HM weight begins to decrease, to a value of where approximately 25% of HM liquid remains in the ladle, simulated results provide a close approximation of the real process. After this point, a decline in accuracy can be seen, where a significant discrepancy between simulated and real weight values is present. This, in turn, increases the average error to 4.1%. One possible explanation for this is that at this point, due to low remaining volumes of liquid, flow resistance coefficient will decrease due to liquid metal adherence to the ladle walls. Here, semi-liquidous metallic slag can also be present, decreasing the overall viscosity of the mix. Refractory degradation is non-linear, meaning that pooling effect can be formed, trapping remaining HM inside refractory cavities. This will increase flow resistance in this pouring region and require for ladles to be rotated to higher angles, to ensure remaining HM is poured out.

Deviations in simulated results can reduce the effectiveness of the model, specifically where close pouring control is required. For example, in metal casting industries, flow deviations in pouring metal into moulds can cause defects. Using this DT, some deviations in resultant HM flow rate are expected, between simulated and actual results, due to disparities caused by unknown process conditions seen towards the end of HM pouring. However, quality of steel produced using the BOS method would not be impacted by changes in the HM flow rates. In addition, if this model was to be applied to test a feed-forward controlled HM pouring movement, end of pouring deviations seen here would result in a

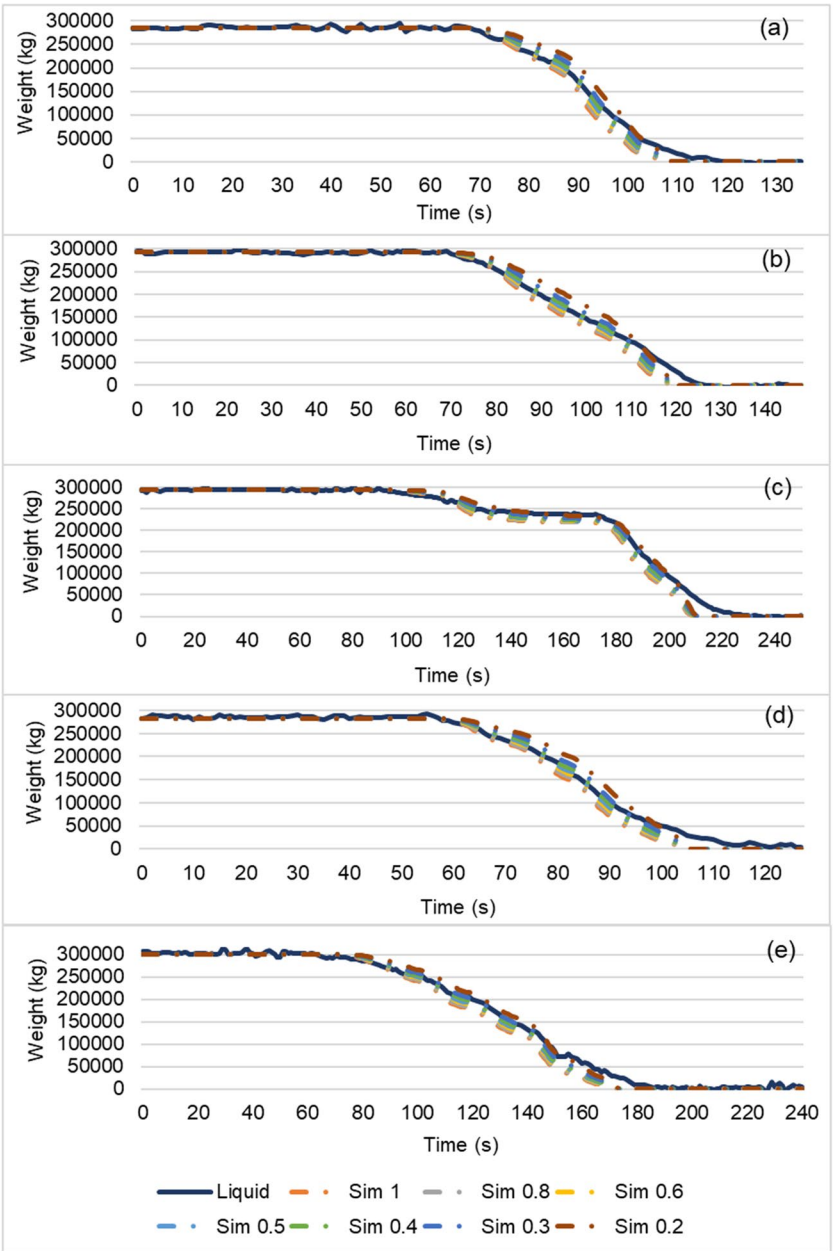

Fig. 14 Comparison of simulation results and measured liquid HM weight. **a** Test 1, **b** Test 2, **c** Test 3, **d** Test 4 and **e** Test 5

Table 3 Simulation comparison with measured weight data: best match flow coefficient and resultant error value

Test No.	Flow constant	Error %
Test 1	0.3	4.79
Test 2	0.4	4.18
Test 3	0.2	3.19
Test 4	0.4	4.79
Test 5	0.3	3.54
Average	0.32	4.1

decrease of HM pouring rates, due to additional resistance to flow in the ladles. This should not impact the release of thermal emissions as this is influenced by increase in pouring rates [5, 6].

Using rational that heat emissions are released due to mixing of scrap with HM where trapped moisture evaporates and impurities are burned off, at 75% mark, > 200 t of HM would have been already poured into the vessel, allowing for the mixing of HM with scrap to take place. Therefore, likelihoods of large thermal releases in this final region would also be reduced, since mixing of scrap with HM would have already taken place, removing the need for close HM transfer rate controls.

Table 4 Simulation error with 0.32 flow constant

Test No.	Error %; 0.32 flow constant
Test 1	4.30
Test 2	4.74
Test 3	3.44
Test 4	5.01
Test 5	3.57
Average	4.21

5.1 Flow model calibration

To reduce possible variations in simulation results due to unknown ladle and process conditions, flow resistance coefficient value in the model was calibrated using the average value of 0.32. Table 4 displays error match percentage value for the 5 tests, using $c = 0.32$. Marginal increase in the error value is seen for tests 2, 3 and 5. Error value decreases for tests 1 and 4. The average error increases to a value of 4.21%. With an average increase of 0.11%, this value is seen as acceptable to be used in the model.

6 Conclusions

In this paper a DT model is outlined for a HM charging system, incorporating a model for an overhead gantry charging crane and a HM ladle. This model combines the use of MBD and dynamic system modelling to model the rigid body movement of mechanical components and to predict flow rate of liquid metal during ladle rotation motion. The main findings are as follows:

- A friction estimation model, based on joint geometry and material properties, was developed to account for friction losses in revolute joint components. Resultant frictional reaction torque was determined by applying a Velocity based estimation model, using the MBD model to simulate angular joint velocities. Forces, acting on these joints, were estimated as functions of changing load weight, present due to pouring of HM. Both mass and the applied forces were estimated based on the ladle tilting angle. This provides a unique modelling solution using dynamic force inputs to estimate friction losses. Finally, the frictional torque estimation model was applied to the movement damping of the system.
- A dynamic system model was applied to estimate the flow of HM. This model was incorporated with the MBD and frictional torque estimation models. The resultant DT of the HM charging system was verified by simulating real crane and ladle movement and by making a comparison between simulated and recorded HM weights. The average error deviation showed to be 4.21%, accurately conveying crane and ladle movement for prediction of HM flow rate.
- A reduction in model accuracy is found due to a discrepancy between simulated and measured HM weights towards the end of HM charges. This is theorised to be due to a reduction of flow resistance coefficient and build-up of metallic slag, where metal adheres to the walls of the ladle.
- Overall, the devised DT model can be used for flow rate estimation using accurate crane movement. This can be applied in testing of different ladle movements and controlled pouring schemes, providing a safe testing environment and removing the need for the creation of physical models.
- The presented pouring movement testing method is transferable to other pouring systems, where safety is a concern due to size or fluid medium involved. MBD model for the mechanical system would need to be created, to accurately depict system movement and the dynamic flow prediction model would need to be adapted for different ladle/vessel dimensions and liquid properties.

Acknowledgements The authors would like to acknowledge the M2A funding from the European Social Fund via the Welsh Government (c80816) and Tata Steel UK that have made this research possible.

Author contribution IP: Conseptualisation, research, methodology, data collection, model development, analysis and writing of original manuscript. CAG: Consepsualisaion, supervision, manuscript review and editing. All authors read and approved the final manuscript.

Funding This research was conducted with M2A funding from the European Social Fund via the Welsh Government (c80816) and support from Tata Steel UK.

Declarations

Conflict of interest The authors declare no competing interests.

References

1. Popov V, Gabtykaev D (2008) Cables with a steel core for hot-metal charging cranes. Metallurgist 52(9–10):588–591. https://doi.org/10.1007/s11015-009-9097-4
2. Popov V, Kabakov Z, Gabtykaev D (2009) Mathematical modeling of the heating of the metal structures of a foundry crane

equipped with heat shields. Metallurgist 53(11–12):704–709. https://doi.org/10.1007/s11015-010-9236-y
3. Maslov V (2004) Vlijanie termociklicheskih vozdejstvij rasplavlennogo metalla na sistemu konverter-kran i sovershenstvovanie ee jelementov [Influence of thermocyclic actions of molten metal on the converter - crane system and imporvements of its elements]. Doctoral dissertation, Cherepovets State University. DisserCat. https://www.dissercat.com/content/vliyanie-termotsiklicheskikh-vozdeistvii-rasplavlennogo-metalla-na-sistemu-konverter-kran-i-
4. Enviromental A (2004) Integrated Pollution Prevention and Control (IPPC) Guidance for the production of Coke, Iron and Steel. Enviromental Agency, Bristol
5. Miller TW, Jimenez J, Sharan A, Goldstein DA (1998) Oxygen steelmaking process. In: Fruehan RJ (ed) The making, shaping and Treating of Steel, steelmaking and refining volume. AISE Steel Foundation, Pittsburgh, PA, pp 475–524
6. Popov I, Todeschini G (2022) Flame intensity analysis for hot molten metal pouring in the steel industry by applying image segmentation. Advances in Manufacturing processes, Intelligent methods and systems in Production Engineering. Springer International Publishing, Cham, pp 632–646. https://doi.org/10.1007/978-3-030-90532-3_47
7. Sugimoto Y, Yano K, Terashima K (2002) Liquid level control of automatic pouring robot by two-degrees-of-freedom control. IFAC Proc 35(1):137–142. https://doi.org/10.3182/20020721-6-ES-1901.01174
8. Noda Y, Yano K, Terashima K (2005) Control of self-transfer-type automatic pouring robot with cylindrical ladle. IFAC Proc 38(1):295–300. https://doi.org/10.3182/20050703-6-CZ-1902.01471
9. Noda Y, Terashima K (2006) Nonlinear modeling with Hydrodynamics and Flow Control using Inverse Pouring dynamics of Tilding-Ladle-Type Automatic pouring process. 67th World Foundry Congress, Harrogate, UK, June 5–7 2006, vol 1. Institute of Cast Metals Engineers (ICME), pp 51–60
10. Matsuo Y, Noda Y, Terashima K, Hashimoto K, Suzuki Y (2006) Modeling and identification of pouring Flow process with tilting-type ladle for an innovative press casting Method using Greensand Mold. 67th World Foundry Congress, Harrogate, UK, 5–7 June 2006, vol 1. Institute of Cast Metals Engineers (ICME), pp 493–502
11. Noda Y, Terashima K (2007) Modeling and Feedforward Flow Rate Control of Automatic Pouring System with Real Ladle. J Robot Mechatron 19(2):205–211. https://doi.org/10.20965/jrm.2007.p0205
12. Noda Y, Matsue Y, Terashima K, Zheng Y (2008) A novel flow rate estimation method using extended kalman filter and sensor dynamics compensation with automatic casting pouring process. IFAC Proc 41(2):710–715. https://doi.org/10.3182/20080706-5-KR-1001.00121
13. Noda Y, Terashima K (2009) Estimation of Flow Rate in Automatic pouring system with real ladle used in industry. 2009 ICCAS-SICE, Fukuoka, Japan, August 18–21 2009. Society of Instrument and Control Engineers, pp 354–359
14. Li L, Wang C, Wu H (2018) Research on Kinematics and Pouring Law of a Mobile Heavy load pouring Robot. Math Probl Eng. https://doi.org/10.1155/2018/8790575
15. Terashima K, Yano K, Sugimoto Y, Watanabe M (2001) Position control of ladle tip and sloshing suppression during tilting motion in automatic pouring machine. IFAC Proc 34(18):229–234. https://doi.org/10.1016/S1474-6670(17)33211-1
16. Noda Y, Terashima K (2007) Falling position control of outflow liquid for automatic pouring system with tilting-type ladle. IFAC Proc 40(11):53–58. https://doi.org/10.3182/20070821-3-CA-2919.00009
17. Noda Y, Fukushima R, Terashima K (2010) Monitoring and control system to falling position of outflow liquid in automatic pouring robot. IFAC Proc 43(9):13–18. https://doi.org/10.3182/20100802-3-ZA-2014.00003
18. Ohnishi E, Tsuboi I, Egusa T, Uesugi M (1981) Automatic control of an overhead crane. IFAC Proceedings Volumes 14 (2):1885–1890. https://doi.org/10.1016/S1474-6670(17)63747-9
19. Moustafa KA, Ebeid AM (1988) Nonlinear modeling and control of overhead crane load sway. J Dyn Sys Meas Control 110(3):266–271. https://doi.org/10.1115/1.3152680
20. Lee H-H (1998) Modeling and control of a three-dimensional overhead crane. J Dyn Sys Meas Control 120(4):471–476. https://doi.org/10.1115/1.2801488
21. Jones JF, Petterson BJ (1988) Oscillation damped movement of suspended objects. In: Proceedings. 1988 IEEE International Conference on Robotics and Automation. IEEE, pp 956–962. https://doi.org/10.1109/ROBOT.1988.12183
22. Yusop AM, Mohamed Z, Sulaiman NA (2008) Inverse dynamic analysis with feedback control for vibration-free positioning of a gantry crane system. In: 2008 International Conference on Electronic Design, 2008. IEEE, Panang, Malaysa, pp 1–5. https://doi.org/10.1109/ICED.2008.4786664
23. Jaafar HI, Mohamed Z, Jamian J, Abidin AFZ, Kassim AM, Ab Ghani Z (2013) Dynamic behaviour of a nonlinear gantry crane system. Proc Technol 11:419–425. https://doi.org/10.1016/j.protcy.2013.12.211
24. Solihin MI, Wahyudi, Legowo A (2010) Fuzzy-tuned PID anti-swing control of automatic gantry crane. J Vib Control 16(1):127–145. https://doi.org/10.1177/1077546309103421
25. Maghsoudi M, Mohammed Z, Pratiwi A, Ahmad N, Husain A (2012) An experiment for position and sway control of a 3D gantry crane. In: 2012 4th International Conference on Intelligent and Advanced Systems (ICIAS2012), 2012. IEEE, pp 497–502. https://doi.org/10.1109/ICIAS.2012.6306066
26. Lévine J (1999) Are there new industrial perspectives in the control of mechanical systems? Advances in control: highlights of ECC'99. Springer, pp 197–226. doi:https://doi.org/10.1007/978-1-4471-0853-5_7
27. Zhang L, Qin Y, Wang Y (2021) Risk assessment and intelligent control of ladle pouring mechanism. J Fail Anal Prev 21:904–913. https://doi.org/10.1007/s11668-021-01133-7
28. MathWorks (2023) MATLAB. In: MathWorks. https://www.mathworks.com/products/matlab.html. Accessed 20/08 2023
29. Scientific Computing World (2023) Multibody simulation drives dynamic system design. In: Scientific Computing World. https://www.scientific-computing.com/feature/multibody-simulation-drives-dynamic-system-design. Accessed 20/03 2023
30. Kim H, Oh K, Ko K, Kim P, Yi K (2016) Modeling, validation and energy flow analysis of a wheel loader. J Mech Sci Technol 30:603–610. https://doi.org/10.1007/s12206-016-0114-9
31. He B, Tang W, Cao J (2014) Virtual prototyping-based multibody systems dynamics analysis of offshore crane. Int J Adv Manuf Tech 75:161–180. https://doi.org/10.1007/s00170-014-6137-4
32. Li K, Liu M, Yu Z, Lan P, Lu N (2022) Multibody system dynamic analysis and payload swing control of tower crane. Proc Inst Mech Eng, Part K: J Multi-body Dyn 236(3):407–421. https://doi.org/10.1177/1464419322110199
33. Cha J-H, Roh M-I, Lee K-Y (2010) Dynamic response simulation of a heavy cargo suspended by a floating crane based on multibody system dynamics. Ocean Eng 37(14–15):1273–1291. https://doi.org/10.1016/j.oceaneng.2010.06.008
34. Rouvinen A, Lehtinen T, Korkealaakso P (2005) Container gantry crane simulator for operator training. Proc Inst Mech Eng, Part K: J Multi-body Dyn 219(4):325–336. https://doi.org/10.1243/146441905X63322

35. Hung W-H, Kang S-C (2013) Configurable model for real-time crane erection visualization. Adv Eng Softw 65:1–11. https://doi.org/10.1016/j.advengsoft.2013.04.013
36. MathWorks (2023) Simulink. In: MathWorks. https://www.mathworks.com/products/simulink.html. Accessed 03/03/ 2023
37. MathWorks (2023) Simscape. In: MathWorks. https://www.mathworks.com/products/simscape.html. Accessed 06/08 2023
38. MathWorks (2023) Simscape multibody. In: MathWorks. https://www.mathworks.com/products/simscape-multibody.html. Accessed 06/08 2023
39. Dassault S (2023) SOLIDWORKS 3D CAD. In: SolidWorks. https://www.solidworks.com/product/solidworks-3d-cad. Accessed 04/08 2023
40. Dassault Systems (2023) Simscape multibody link. In: SolidWorks. https://www.solidworks.com/partner-product/simscape-multibody-link. Accessed 20/03 2023
41. Olsson H, Åström KJ, De Wit CC, Gäfvert M, Lischinsky P (1998) Friction models and friction compensation. Eur J Control 4(3):176–195. https://doi.org/10.1016/S0947-3580(98)70113-X
42. Marques F, Flores P, Claro JP, Lankarani HM (2019) Modeling and analysis of friction including rolling effects in multibody dynamics: a review. Multibody Syst Dyn 45:223–244. https://doi.org/10.1007/s11044-018-09640-6
43. Pennestrì E, Rossi V, Salvini P, Valentini PP (2016) Review and comparison of dry friction force models. Nonlinear Dyn 83:1785–1801. https://doi.org/10.1007/s11071-015-2485-3
44. Coulomb CA (1821) Théorie Des machines simples en ayant égard Au frottement de leurs parties et à La Roideur Des cordages [Theory of simple machines taking into account the friction of their parts and the stiffness of the ropes]. Bachelier, Paris, France
45. Brown P, McPhee J (2016) A continuous velocity-based friction model for dynamics and control with physically meaningful parameters. J Comput Nonlinear Dyn 11(5):054502. https://doi.org/10.1115/1.4033658
46. Benson DJ, Hallquist JO (1990) A single surface contact algorithm for the post-buckling analysis of shell structures. Comput Methods Appl Mech Eng 78(2):141–163. https://doi.org/10.1016/0045-7825(90)90098-7
47. Armstrong-Helouvry B (2012) Control of machines with friction. The Springer International Series in Engineering and Computer Science, vol 128. Springer Science & Business Media, New York, NY
48. Makkar C, Dixon W, Sawyer W, Hu (2005) G A new continuously differentiable friction model for control systems design. In: Proceedings, 2005 IEEE/ASME International Conference on Advanced Intelligent Mechatronics., IEEE, pp 600–605. https://doi.org/10.1109/AIM.2005.1511048
49. Faraz A, Payandeh S (2000) Engineering approaches to mechanical and robotic design for minimally invasive surgery (MIS). The Springer International Series in Engineering and Computer Science, vol 454. Springer Science & Business Media. https://doi.org/10.1007/978-1-4615-4409-8. Ney York, NY. doi
50. Lipson C, Juvinall RC (1963) Handbook of stress and strength: design and material applications. Macmillan, New York, NY
51. Miller S (2023) Simscape multibody multiphysics library. GitHub. https://github.com/mathworks/Simscape-Multibody-Multiphysics-Library/releases/tag/23.1.4.1. Accessed 06/12 2023
52. Yang H, Qin Y, Ren J, Gu J (2021) Analysis of casting hook load on ladle crane. J Fail Anal Prev 21:338–344. https://doi.org/10.1007/s11668-020-01075-6
53. The Engineering Toolbox (2004) Friction - friction coefficients and calculator. In: The Engineering Toolbox. https://www.engineeringtoolbox.com/friction-coefficients-d_778.html. Accessed 23/11 2023
54. Barrett RT (1990) Fastener design manual. NASA Lewis Research Centre, Cleveland, OH
55. Eurocode Applied (2022) Table of design material properties for structural steel. In: Eurocode Applied. https://eurocodeapplied.com/design/en1993/steel-design-properties. Accessed 20/11 2022
56. Weisstein EW (2002) Circular segment. In: MathWorld Wolfram. https://mathworld.wolfram.com/CircularSegment.html. Accessed 19/12 2023